New Journal of Chemistry **2021**, *45*, 4427-4436

https://doi.org/10.1039/D1NJ00254F

ARTICLE

Group VIII Coordination Complexes of Bidentate *P^N* Ligands Bearing π-Extended Quinoline or Phenanthridine *N*-Heterocycles

Received 00th January 20xx,
Accepted 00th January 20xx

DOI: 10.1039/x0xx00000x

Rajarshi Mondal[a], Jason D. Braun[a], Issiah B. Lozada[a], Rachel Nickel[b], Johan van Lierop[b,c], David E. Herbert[a,c]*

A series of Fe and Ru coordination complexes supported by bidentate *P^N* ligands bearing π-extended phenanthridine (3,4-benzoquinoline; $^{Phen}L^{R,R'}$) or quinoline ($^{Quin}L^{H,Ph}$) *N*-heterocycles have been synthesized and fully characterized. Tetrahedral monomeric (*P^N*)$FeBr_2$ and trigonal bipyramidal dimeric ((*P^N*)$FeBr)_2(\mu\text{-}Br)_2$ complexes were found to be high-spin paramagnets as solids (magnetic susceptibility balance measurements) and in solution (Evans method), while *tris*-ligated octahedral $[(P\text{^}N)_3M]^{2+}$ cations (M = Fe, Ru) are low-spin diamagnets. The electronic environment about each Fe centre was further examined by Mössbauer spectroscopy. The impact of π-extension is evident when comparing the lowest energy absorption bands in the UV-Vis spectra. Contrary to conventional assumptions regarding π-extension, a small hypsochromic shift was observed for the more π-extended phenanthridinyl phosphine-supported Fe(II) complex compared to the analogous quinolinyl complex. Density functional theory (DFT), time-dependent DFT (TDDFT) and charge decomposition analysis (CDA) revealed benzannulation most significantly impacts the character of the lowest energy excitation, rather than significantly affecting the energies of the frontier orbitals. The impact of electron-transfer on the electronic absorption properties of the π-extended pseudo-octahedral Fe complexes was further explored by spectroelectrochemistry.

Introduction

Chelating, benzannulated ligands combine strong bonding to metal ions and vacant, low-lying ligand-based orbitals resulting from π-extension. They can therefore enable intense low energy electronic excitations with charge-transfer character in their coordination complexes. The typical impact of extending π-conjugation in a ligand system is to induce bathochromic shifts of absorption and emission bands, as the frontier orbitals become progressively closer in energy.[1,2] For example, $Ir(piq)_3$ (piq = 1-phenylisoquinolinato) shows distinctly red-shifted emission compared with $Ir(ppy)_3$ (ppy = 2-phenylpyridinato).[3] This effect, however, is not universal and examples of both transition metal coordination complexes[4–7] and organic molecules[8] have been reported that challenge the extent to which this conventional view is broadly applicable. These exceptions have been interpreted not only in terms of the impact of site-selective π-extension on frontier molecular orbital energies and the corresponding changes to the lowest lying singlet (S_1) and triplet (T_1) excited states,[8] but also through the impact of π-extension on molecular rigidity.[9,10] There can be other consequences to adjusting the size of a ligand π-system as well. For example, incorporation of quinolinyl, naphthyl and anthracenyl groups in cyclometallating ligands derived from 2,6-di(quinolin-8-yl)pyridine provides adjustable bite angles that help engender extended excited state lifetimes in Ru(II) polypyridyl-type complexes.[11]

Compared with ligands bearing moieties derived from π-extended units such as quinoline or phenanthroline, incorporation of phenanthridine (3,4-benzoquinoline) into ligand motifs has been less well-explored. Some of the few example systems include *C^N*-cyclometallated phenanthridine-supported Pt[12] and Ir[13] phosphors. In the latter case, deep-red phenanthridinyl-containing Ir(III) emitters were used in the construction of highly efficient solution-processed LEDs.[13] Phenanthridines have also been incorporated into tridentate, pincer-like diarylamido frameworks and used to form iron(II) coordination complexes with nanosecond charge-transfer excited state lifetimes[14], and platinum complexes with some of the deepest red phosphorescence thus far reported from mononuclear emitting states.[15] Here, we present a series of Group VIII coordination complexes made of simpler phenanthridinyl- and quinolinyl-containing bidentate *P^N* ligands, and discuss their structural and photophysical characterization. Ligand benzannulation – specifically comparing quinolinyl vs. phenanthridinyl *N*-heterocyclic donors – was found to impact the properties of these complexes in a unique manner compared to previously reports.

[a] *Department of Chemistry, University of Manitoba, 144 Dysart Rd, Winnipeg, MB, R3T 2N2, Canada; *david.herbert@umanitoba.ca*
[b] *Department of Physics and Astronomy, University of Manitoba, 31A Sifton Rd, Winnipeg, MB, Canada, R3T 2N2*
[c] *Manitoba Institute for Materials, University of Manitoba, 20 Sifton Rd, Winnipeg, MB, Canada, R3T 2N2*

Electronic Supplementary Information (ESI) available: Full experimental details on the synthesis and characterization of all new complexes; tables of bond distances and angles; tabulated redox and electronic absorption parameters; computational methodology, data tables and figures; multi-nuclear NMR of all new compounds; crystallographic information files containing all X-ray data. See DOI: 10.1039/x0xx00000x

Results and discussion

Proligands (4-diphenylphosphino)phenanthridine ($^{Phen}L^{H,Ph}$),[16] (4-diphenylphosphino-2-methyl)phenanthridine ($^{Phen}L^{Me,Ph}$)[9] and (8-diphenylphosphino)quinoline ($^{Quin}L^{Me,Ph}$)[9] have been previously described. A new variant with more strongly electron-releasing *i*Pr substituents at phosphorus, (4-di-*iso*propyl-phosphino-2-methyl)phenanthridine ($^{Phen}L^{Me,iPr}$), was constructed in a similar fashion and is reported here. Briefly, (2-methyl-4-bromo)phenanthridine[6] was reacted at low temperature with *sec*BuLi and the lithiated intermediate quenched with *i*Pr$_2$PCl (Scheme 1). $^{Phen}L^{Me,iPr}$ was isolated as a yellow solid (63% yield) after passing through a short silica plug using hexane as eluent and characterized by multinuclear (^{1}H, ^{13}C, ^{31}P) NMR spectroscopy. The proligand bears the same structural phenanthridine subunit as $^{Phen}L^{R,Ph}$ (R = H, Me) and thus presents the same imine-like character to the C=N subunit. Accordingly, the hydrogen in the 6-position (*ortho* to the phenanthridine nitrogen) appears as a downfield singlet in the ^{1}H NMR spectrum [δ(C$_6$-*H*) = 9.29 ppm; *cf.* 9.23 ($^{Phen}L^{H,Ph}$) and 9.19 ppm ($^{Phen}L^{Me,Ph}$)]. A downfield resonance attributed to the imine-like carbon nucleus is also observed by ^{13}C{^{1}H} NMR [δ(*C*$_6$-H) = 151.5 ppm; *cf.* 152.8 ($^{Phen}L^{H,Ph}$) and 151.8 ppm ($^{Phen}L^{Me,Ph}$)]. In the ^{31}P{^{1}H} NMR spectrum, a sharp singlet is seen at δ = -0.2 ppm, significantly shifted from the corresponding resonance for $^{Phen}L^{H,Ph}$ (-13.7 ppm) or $^{Phen}L^{Me,Ph}$ (-13.6 ppm), as a result of exchanging phenyl substituents for alkyl groups.

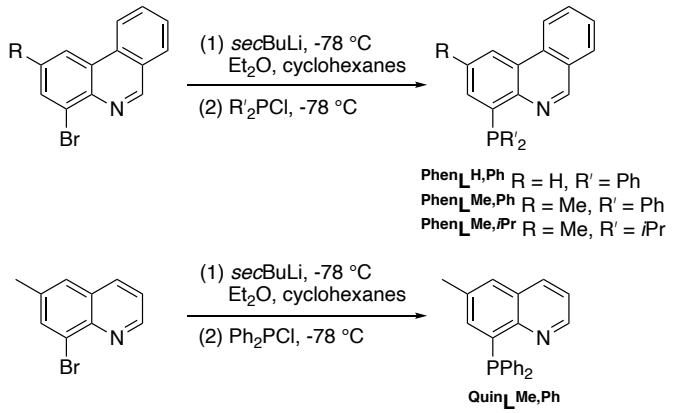

Scheme 1. Bidentate *P^N* proligands.

P^N-ligated coordination complexes of Fe(II) were then synthesized via drop-wise addition of CH_2Cl_2 solutions of the appropriate proligand to suspensions of $FeBr_2$ in THF (Scheme 2). The ^{1}H NMR spectra shifts of all three products were broad and uninformative, consistent with their paramagnetism. The NMR spectra were nevertheless quite uniform, suggesting similar structures are adopted in solution. For example, the chemical shift range of paramagnetically shifted peaks observed in the ^{1}H NMR spectrum of (($^{Phen}L^{H,Ph}$)FeBr)$_2$(μ-Br)$_2$ extended from +23.20 to -7.98 ppm, while for ($^{Phen}L^{Me,Ph}$)FeBr$_2$ the range was +22.64 to -8.19 ppm, and for ($^{Phen}L^{Me,iPr}$)FeBr$_2$ +25.56 to -9.79 ppm (see Supporting Information). Neither ^{13}C nor ^{31}P NMR signals were detectable. Note, for simplicity we refer to the products of these reactions using formulae consistent with their solid-state structures (*vide infra*).

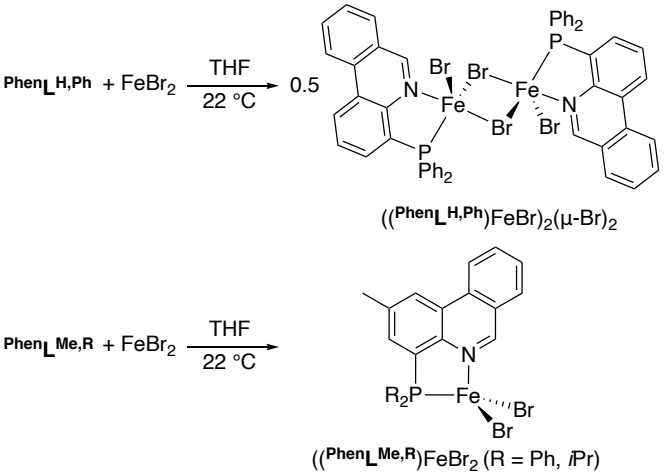

Scheme 2. Synthesis of paramagnetic (*P^N*)FeBr$_2$ complexes.

The solid-state structures of all three complexes were determined via X-ray diffraction using single crystals grown by slow diffusion of hexanes into CH_2Cl_2 solutions of each material. A dimeric structure was observed for orange plates of (($^{Phen}L^{H,Ph}$)FeBr)$_2$(μ-Br)$_2$, while ($^{Phen}L^{Me,Ph}$)FeBr$_2$ and ($^{Phen}L^{Me,iPr}$)FeBr$_2$ both crystallized as yellow blocks with monomeric structures (Figure 1). For the dimeric (($^{Phen}L^{H,Ph}$)FeBr)$_2$(μ-Br)$_2$, each iron centre is five-coordinate with a τ_5 value of 0.64, representative of a distorted trigonal bipyramidal-type geometry.[17] However, one Fe-Br interaction with one of the two bridging halides is particularly long [2.728(1) Å] compared with both the second bridging Br-Fe contact [2.474(1) Å] and the terminal Br(2)–Fe(1) bond distance [2.378(1) Å]. While this longer distance is still certainly within the range of a meaningful bonding interaction, it does suggest dimer dissociation into individual pseudo-tetrahedral ($^{Phen}L^{H,Ph}$)FeBr$_2$ units is possible.

Indeed, the magnetic moments calculated from in solution measurements using Evans method[18] (corrected for the appropriate diamagnetic contributions[19]) for the three complexes are quite similar [(($^{Phen}L^{H,Ph}$)FeBr)$_2$(μ-Br)$_2$ 4.40μ_B; ($^{Phen}L^{Me,Ph}$)FeBr$_2$ 4.47μ_B; ($^{Phen}L^{Me,iPr}$)FeBr$_2$ 4.86μ_B] as befits four unpaired electrons in a high-spin Fe(II) d^6 system. Solid-state magnetic susceptibility measurements using dry powders gave similar values: [(($^{Phen}L^{H,Ph}$)FeBr)$_2$(μ-Br)$_2$ 4.25μ_B; ($^{Phen}L^{Me,Ph}$)FeBr$_2$ 4.35μ_B; ($^{Phen}L^{Me,iPr}$)FeBr$_2$ 4.30μ_B]. In addition, UV-Vis absorption spectra collected in dichloromethane solution for the series are also nearly identical (*vide infra*), consistent with the presence of similar electronic environments about each iron centre.

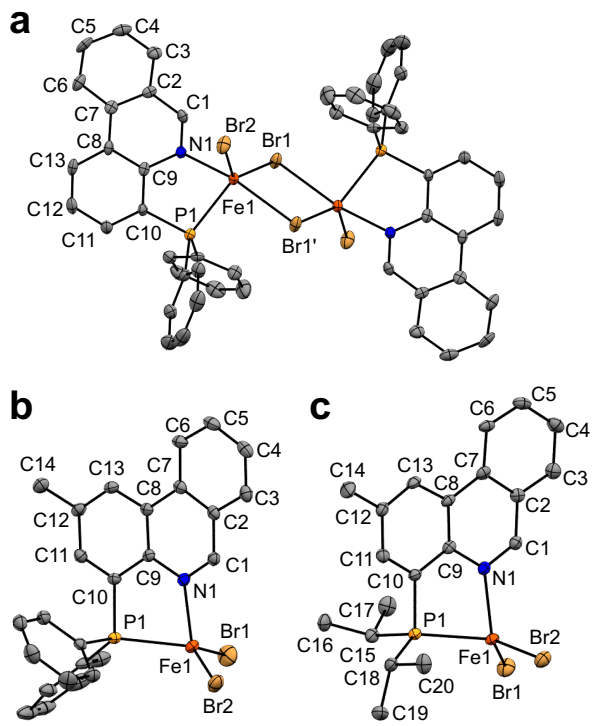

Figure 1. Solid-state structures of (a) $(^{Phen}L^{H,Ph})FeBr_2)_2(\mu\text{-}Br)_2$, (b) $(^{Phen}L^{Me,Ph})FeBr_2$ and (c) $(^{Phen}L^{Me,iPr})FeBr_2$ shown with thermal ellipsoids at 50% probability levels. Hydrogen atoms, solvent molecules and phenyl carbon labels are omitted for clarity. Selected bond distances (Å) and angles (°) for $(^{Phen}L^{H,Ph})FeBr_2)_2(\mu\text{-}Br)_2$: Br1–Fe1 2.47384(10), Br1'–Fe1 2.7277(10), Br2–Fe1 2.3777(10), N1–Fe1 2.227(4), P1–Fe1 2.4210(16), N1–C1 1.290(6); Fe1-Br1-Fe1 93.76(3), N1-Fe1-P1 76.27(11), P1-Fe1-Br2 114.19(5), N1-Fe1-Br2 94.17(11), N1-Fe1-Br1 91.10(11). $(^{Phen}L^{Me,Ph})FeBr_2$: N1–Fe1 2.1075(16), P1–Fe1 2.4183(6), Br1–Fe1 2.3592(4), Br2–Fe1 2.3704(4), N1–C1 1.309(3); N1-Fe1-Br1 111.39(5), N1-Fe1-Br2 108.51(5), N1-Fe1-P1 79.54(5), P1-Fe1-Br1 107.773(18), P1-Fe1-Br2 119.570(18). $(^{Phen}L^{Me,Ph})FeBr_2$: N1–Fe1 2.123(2), P1–Fe1 2.4210(8), Br1–Fe1 2.3702(5), Br2–Fe1 2.3689(5), N1–C1 1.310(3); N1-Fe1-Br1 111.42(6), N1-Fe1-Br2 109.30(6), N1-Fe1-P1 80.40(6), P1-Fe1-Br1 118.24(2), P1-Fe1-Br2 113.21(2).

Pseudo-octahedral *tris*-ligated Fe complexes of $^{Phen}L^{Me,Ph}$ and $^{Quin}L^{Me,Ph}$ were prepared using an appropriate source of Fe(II) and three equivalents of proligand in the absence of more strongly bonding halide counterions (Scheme 3a-b). The resulting complexes were precipitated from deep red reaction mixtures as dark orange-brown solids with either hexafluorophosphate or tetraphenylborate salts, and purified via recrystallization from mixtures of CH_2Cl_2 and diethylether. $[(^{Phen}L^{Me,Ph})_3Fe][PF_6]_2$ and $[(^{Quin}L^{Me,Ph})_3Fe][X]_2$ (X = PF_6, BPh_4) were characterized in solution using 1- and 2D ^1H, ^{13}C and $^{31}P\{^1H\}$ NMR spectroscopy and in the solid-state via single crystal X-ray (Figure 2). Both octahedral Fe(II) complexes are diamagnetic with symmetric binding environments for each ligand evidenced by the symmetric multinuclear NMR spectra. The solid-state structured revealed a 'facial' arrangement of the *P^N* ligands for both ligand sets. For $[(^{Quin}L^{Me,Ph})_3Fe]^{2+}$, higher quality crystals could be grown only in combination with BPh_4^- counterions. Both structures contain cations significantly distorted from a perfect octahedral geometry that results from constrained *P^N* ligand bite angles (~82-83°). The presence of phenyl substituents at each phosphorus donor further widens the P-Fe-P angles (~100°); the inter-ligand N-Fe-N angles are in fact quite close to 90°.

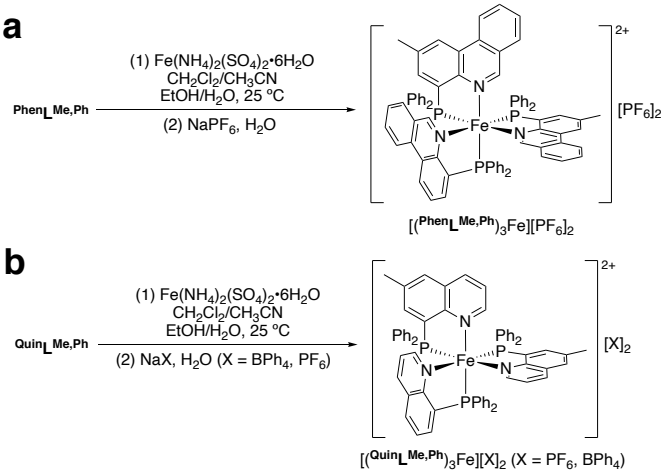

Scheme 3. Synthesis of diamagnetic pseudo-octahedral $[(P^N)_3Fe]^{2+}$ complexes of (a) $^{Phen}L^{Me,Ph}$ and (b) $^{Quin}L^{Me,Ph}$.

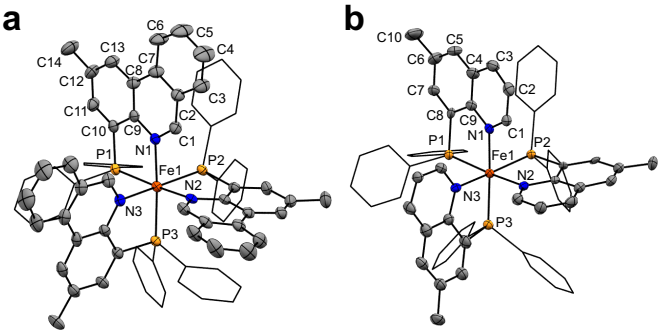

Figure 2. Solid-state structures of the $[(P^N)_3Fe]^{2+}$ dication of (a) $[(^{Phen}L^{Me,Ph})_3Fe][PF_6]_2$ and (b) $[(^{Quin}L^{Me,Ph})_3Fe][BPh_4]_2$. Selected bond distances (Å) and angles (°) for $[(^{Phen}L^{Me,Ph})_3Fe][PF_6]_2$: Fe1–N1 2.086(5), Fe1–N2 2.075(5), Fe1–N3 2.087(5), Fe1–P1 2.2948(16), Fe1–P2 2.2974(17), Fe1–P3 2.2921(17); N1–Fe1–P1 82.52(13), N2–Fe1–P2 82.49(14), N3–Fe1–P3 83.40(14), N1–Fe1–N2 89.97(18), P1–Fe1–P2 100.79(6), N1–Fe1–P2 86.88(13), N1–Fe1–P3 171.75(14). $[(^{Quin}L^{Me,Ph})_3Fe][BPh_4]_2$: N1–Fe1 2.065(5), N2–Fe1 2.063(5), N3–Fe1 2.054(5), P1–Fe1 2.2837(19), P2–Fe1 2.3014(18), P3–Fe1 2.2808(18), N1–C1 1.320(8), N2–C23 1.321(8), N3–C45 1.322(8); N1-Fe1-P3 173.35(14), N2-Fe1-P1 171.39(16), N3-Fe1-P2 172.02(16), N1-Fe1-P1 83.97(15), N2-Fe1-P2 84.81(15), N3-Fe1-P3 83.45(15).

Isostructural complexes of the second-row metal ruthenium $[(^{Phen}L^{Me,Ph})_3Ru][PF_6]_2$ and $[(^{Quin}L^{Me,Ph})_3Ru][PF_6]_2$ were prepared in a similar fashion to analogous pseudo-octahedral Ru(II) complexes of 8-(dimethylphosphino)quinoline (Scheme 4).[20] First, *cis*-$(DMSO)_4RuCl_2$ was mixed with one equivalent of either $^{Phen}L^{Me,Ph}$ or $^{Quin}L^{Me,Ph}$ in $CHCl_3$ and heated in an oil bath set to 85 °C for 2 h. A red solid was isolated in both cases from the reaction mixture at this stage. For $^{Phen}L^{Me,Ph}$, $^{31}P\{^1H\}$ NMR spectroscopy showed two species that were assigned as $(^{Phen}L^{Me,Ph})Ru(DMSO)_2Cl_2$ and $(^{Phen}L^{Me,Ph})_2RuCl_2$ by virtue of their $^{31}P\{^1H\}$ NMR resonances (singlet at 56 ppm; doublets at 64 and 55 ppm, $^2J_{PP}$ = 36 Hz) and high-resolution mass spectrometry (HR-MS). The small coupling constant suggests a *cis* orientation of the phosphine nuclei of the two ligand equivalents in $(^{Phen}L^{Me,Ph})_2RuCl_2$. For $^{Quin}L^{Me,Ph}$ a sole singlet at 56 ppm was observed, indicating formation of $(^{Phen}L^{Me,Ph})Ru(DMSO)_2Cl_2$ as

the lone product. In both cases, addition of two further equivalents of *P^N* ligand and heating to 200 °C for an extended time (2 d) in ethylene glycol produced orange solutions of the desired *tris*-ligated products that could be precipitated as PF_6^- salts. Recrystallization of the mixture of ($^{Phen}L^{Me,Ph}$)Ru(DMSO)$_2$Cl$_2$ and ($^{Phen}L^{Me,Ph}$)$_2$RuCl$_2$ from a CH_2Cl_2/ diethylether provided single crystals of ($^{Phen}L^{Me,Ph}$)$_2$RuCl$_2$ of sufficient quality for X-ray diffraction analysis. In the solid-state, the *cis* orientation of the two phosphine nuclei suggested from the ^{31}P NMR spectrum is evident, and the two phenanthridinyl moieties of the $^{Phen}L^{Me,Ph}$ ligands are orthogonal (Figure 3).

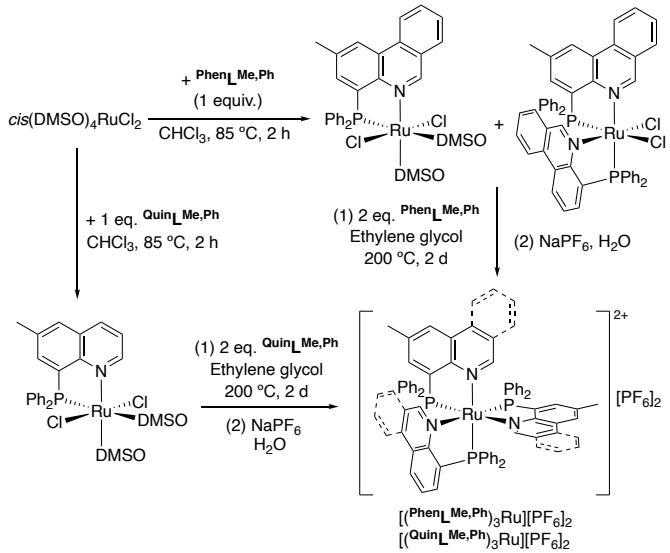

Scheme 4. Synthesis of diamagnetic pseudo-octahedral [(*P^N*)$_3$Ru]$^{2+}$ complexes of $^{Phen}L^{Me,Ph}$ and $^{Quin}L^{Me,Ph}$ and proposed intermediates.

The solution absorption spectra of all seven products were collected and are shown in Figure 4 with results in Table 1. As noted above, the UV-Vis absorption spectra for the series (($^{Phen}L^{H,Ph}$)FeBr)$_2$(μ-Br)$_2$, ($^{Phen}L^{Me,Ph}$)FeBr$_2$ and ($^{Phen}L^{Me,iPr}$)FeBr$_2$ are nearly identical, consistent with similar electronic environments about each iron centre in solution. Each complex showed strong absorption in the UV region, with features at 310 and 360 nm attributable to π-π* transitions of the phenanthridinyl moieties,[6] and a weak tail into the visible region. A similar weak, low energy tail was observed for dimeric halide-bridge Cu(I) complexes of $^{Phen}L^{Me,Ph}$.[9] Of these three species, ($^{Phen}L^{Me,iPr}$)FeBr$_2$ exhibited the highest molar absorptivity.

Table 1. Redox potentials and electronic absorption spectral data for the Fe complexes.

Compound	$E_{1/2}$ / V[a]	λ / nm
(($^{Phen}L^{H,Ph}$)FeBr)$_2$(μ-Br)$_2$	-1.85, 0.80, 1.40[b]	360, 310[c]
($^{Phen}L^{Me,Ph}$)FeBr$_2$	-2.04, 0.63, 1.11[b]	360, 320[c]
($^{Phen}L^{Me,iPr}$)FeBr$_2$	0.77[b]	355, 315[c]
[($^{Phen}L^{Me,Ph}$)$_3$Fe][PF$_6$]$_2$	-1.61, 0.82	435, 371, 316[d]
[($^{Quin}L^{Me,Ph}$)$_3$Fe][PF$_6$]$_2$	-1.55, 0.83	449, 312, 282[d]

[a] in CH_3CN with 0.10 M [nBu_4N][PF_6] as the supporting electrolyte using a glassy carbon working electrode and scan rates of 100 mV s^{-1}. Potentials are listed vs. $FcH^{0/+}$. [b] Irreversible. [c] in CH_2Cl_2 at 295 K. [d] in CH_3CN at 295 K.

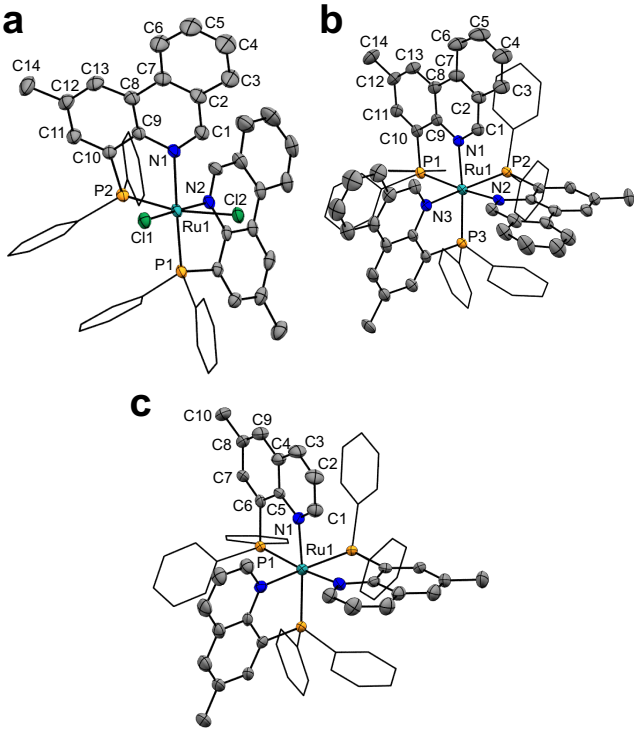

Figure 3. Solid-state structures of (a) [($^{Phen}L^{Me,Ph}$)$_2$RuCl$_2$, (b) the dicationic portion of [($^{Phen}L^{Me,Ph}$)$_3$Ru][PF$_6$]$_2$ and (c) the dicationic portion of [($^{Quin}L^{Me,Ph}$)$_3$Ru][PF$_6$]$_2$ shown with thermal ellipsoids at 50% probability levels. Selected bond distances (Å) and angles (°) for [($^{Phen}L^{Me,Ph}$)$_2$RuCl$_2$: N1-Ru1 2.193(3), N2-Ru1 2.076(3), P1-Ru1 2.2442(8), P2-Ru1 2.2401(8), Cl1-Ru1 2.4238(8), Cl2-Ru1 2.4712(8); N2-Ru1-P1 83.51(7), N2-Ru1-P2 94.08(8), P1-Ru1-Cl1 96.71(3), N1-Ru1-Cl1 83.82(7), P2-Ru1-P1 100.69(3), Cl1-Ru1-Cl2 90.24(3). [($^{Phen}L^{Me,Ph}$)$_3$Ru][PF$_6$]$_2$: N1-Ru1 2.172(4), N2-Ru1 2.188(4), P1-Ru1 2.3193(12), P2-Ru1 2.3166(12), N3-Ru1 2.183(4), P3-Ru1 2.3258(12); N1-Ru1-N2 90.51(15), N1-Ru1-N3 89.53(14), N1-Ru1-P1 80.78(11), N1-Ru1-P2 85.60(11), N1-Ru1-P3 169.81(11), N2-Ru1-P1 171.04(11). [($^{Quin}L^{Me,Ph}$)$_3$Ru][PF$_6$]$_2$: Ru1-P1 2.3129 (12), Ru1-N1(1) 2.178(4); N1-Ru1-P1 81.29(11), N1-Ru1-N1' 89.54(15), P1-Ru1-P1' 101.36(4), P1-Ru1- N1' 87.16(11), P1-Ru1-N1'' 170.28(11).

The pseudo-octahedral [($^{Phen}L^{Me,Ph}$)$_3$Fe][PF$_6$]$_2$ and [($^{Quin}L^{Me,Ph}$)$_3$Fe][PF$_6$]$_2$ complexes, in comparison, both presented a broad, low energy absorption peak in the visible region, with λ_{max} at 435 nm for [($^{Phen}L^{Me,Ph}$)$_3$Fe][PF$_6$]$_2$ and 449 nm for [($^{Quin}L^{Me,Ph}$)$_3$Fe][PF$_6$]$_2$. These absorptions result from metal-to-ligand charge transfer (MLCT) involving the d^6 Fe(II) centres and low-lying vacant orbitals on the *N*-heterocyclic ligand arms. Interestingly, the complex of the more π-extended ligand, [($^{Phen}L^{Me,Ph}$)$_3$Fe][PF$_6$]$_2$, has a λ_{max} at a shorter wavelength. Similar low energy absorptions in the visible region were absent from the spectra of the corresponding second-row complexes, [($^{Quin/Phen}L^{Me,Ph}$)$_3$Ru][PF$_6$]$_2$, which is not entirely unexpected for pseudo-octahedral Ru(II) complexes of *P^N* ligands. For example, while [Ru(bpy)$_3$][PF$_6$]$_2$ (bpy = 6,6'-bipyridyl) exhibits a strong MLCT absorption band centred at 452 nm, analogs where bpy is sequentially replaced by equivalents of $^{Quin}L^{H,Me}$ ($^{Quin}L^{H,Me}$ = (8-dimethylphosphino)quinoline) show increasingly blue-shifted MLCT bands with the *tris-P^N* ligated species not absorbing in the visible at all: [(bpy)$_2$($^{Quin}L^{H,Me}$)Ru][PF$_6$]$_2$, λ_{max} = 423 nm; [(bpy)($^{Quin}L^{H,Me}$)$_2$Ru][PF$_6$]$_2$, λ_{max} = 379 nm; [($^{Quin}L^{H,Me}$)$_3$Ru][PF$_6$]$_2$, λ_{max} = 349 nm.[20] As might be expected, the diamagnetic complexes generally showed stronger absorptivity

values compared the paramagnetic species, consistent with the broader literature on comparable complexes.[21]

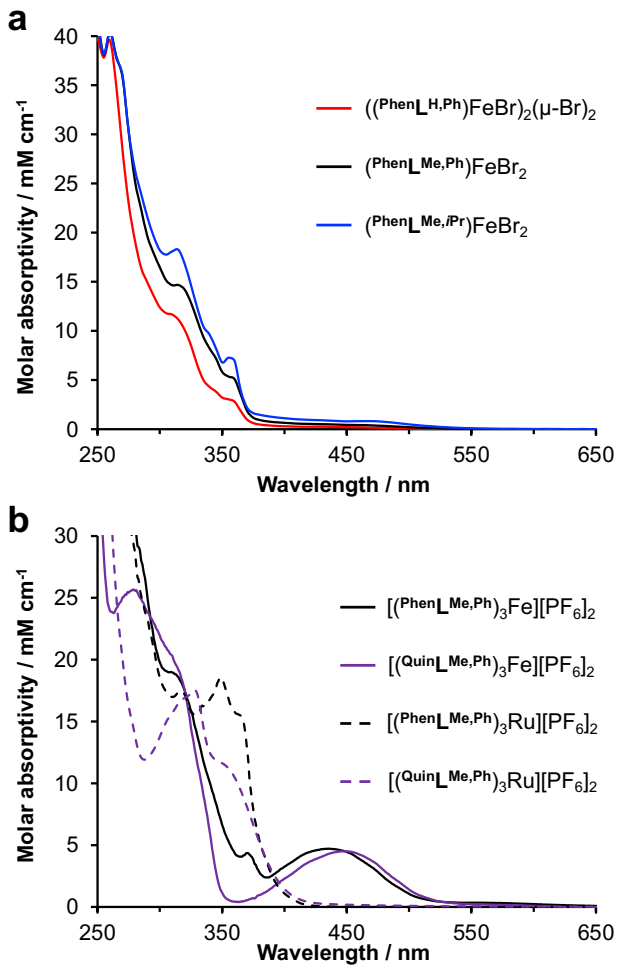

Figure 4. UV-Vis absorption spectra collected at 295 K for (a) $((^{Phen}L^{H,Ph})FeBr)_2(\mu\text{-}Br)_2$, $(^{Phen}L^{Me,Ph})FeBr_2$ and $(^{Phen}L^{Me,iPr})FeBr_2$ in CH_2Cl_2 solution; and (b) $[(^{Phen}L^{Me,Ph})_3M][PF_6]_2$ and $[(^{Quin}L^{Me,Ph})_3M][PF_6]_2$ (M = Fe, Ru) in CH_3CN.

Mössbauer spectra at 10 K were collected for all five Fe(II) complexes in powdered form (Figure 5, Tables 2 and S1). The three high-spin complexes all show isomer shifts (δ) and large quadrupole splittings (ΔE_Q) comparable to values reported for paramagnetic, tetrahedral Fe(II) dihalide complexes of related bidentate ligands.[22,23] The two complexes with monomeric solid-state structures fit well to single sites with consistent line widths. Introduction of more electron-releasing *i*Pr substituents on the ligand phosphine donor arms has the largest impact on the quadrupolar splittings, increasing ΔE_Q for $(^{Phen}L^{Me,iPr})FeBr_2$ compared with $(^{Phen}L^{Me,Ph})FeBr_2$. For $((^{Phen}L^{H,Ph})FeBr)_2(\mu\text{-}Br)_2$, which is dimeric with bridging bromides in the solid state, the spectrum fits with a two-site model (55:45% area ratio). The first component has an identical ΔE_Q to $(^{Phen}L^{Me,Ph})FeBr_2$, while the second spectral component has a larger ΔE_Q than either of the other high-spin complexes. This suggests two Fe environments in the powdered solid sample of $(^{Phen}L^{Me,Ph})FeBr_2$ – one with a similar four-coordinate geometry as $(^{Phen}L^{Me,Ph})FeBr_2$ (consistent with UV-Vis spectroscopic and electrochemical results) and a second with a five-coordinate environment as seen in the solid-state structure.

The δ and ΔE_Q values for the dimer and purported monomer are, however, not that dissimilar. A similar observation was made when comparing the experimental Mössbauer spectra of a structurally related dimer $((SN^H\text{-}Ph_2)FeCl)_2(\mu\text{-}Cl)_2$ supported by a bidentate *N*-(2-pyridyl)amino(diphenylphosphine sulfide) ligand and monomeric analogs.[23] While evidence of a monomeric species was not reported in that instance, the similarity of the ^{57}Fe Mössbauer hyperfine parameters was likewise attributed to only a small change of the coordination geometry of the Fe(II) centre from the formation of a highly asymmetric dimer. For the diamagnetic, low-spin, pseudo-octahedral complexes $[(^{Phen}L^{Me,Ph})_3Fe][PF_6]_2$ and $[(^{Quin}L^{Me,Ph})_3Fe][PF_6]_2$, very similar doublets (and corresponding ΔE_Q's) are observed, although with much broader component linewidth (Γ) for $[(^{Quin}L^{Me,Ph})_3Fe][PF_6]_2$ attributed to inhomogeneities in the crystalline environment. The hyperfine parameters (presented in Tables 2 and S1) from the fits are in agreement with related pseudo-octahedral low-spin, d^6 Fe(II) systems.[24]

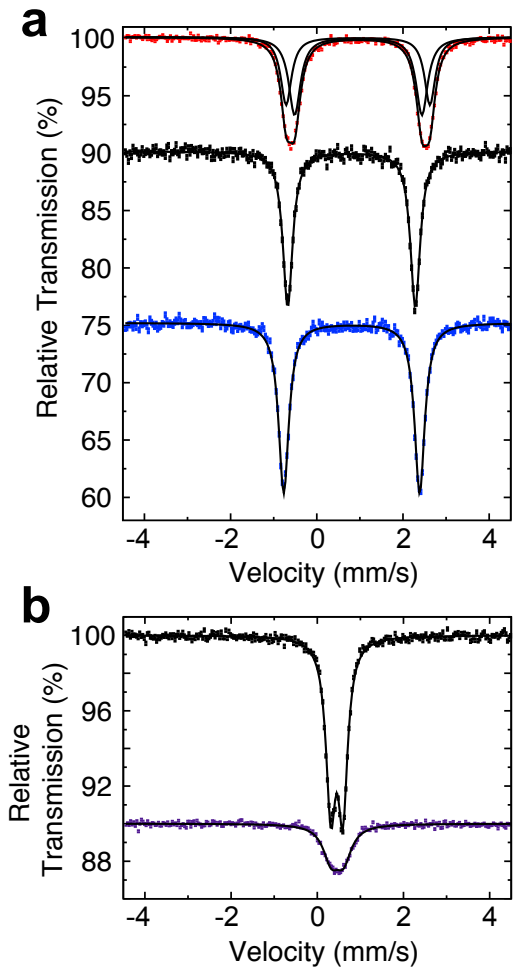

Figure 5. ^{57}Fe Mössbauer spectra (10 K; solid lines represent the fits reported in Table 1) for (a, top to bottom) $((^{Phen}L^{H,Ph})FeBr)_2(\mu\text{-}Br)_2$, $(^{Phen}L^{Me,Ph})FeBr_2$ and $(^{Phen}L^{Me,iPr})FeBr_2$ and (b, top to bottom) $[(^{Phen}L^{Me,Ph})_3Fe][PF_6]_2$ and $[(^{Quin}L^{Me,Ph})_3Fe][PF_6]_2$.

Table 2. ^{57}Fe Mössbauer hyperfine parameters (10 K)

Compound	δ / mm s^{-1}	ΔE_Q / mm s^{-1})
((^{Phen}L^{H,Ph})FeBr)$_2$(μ-Br)$_2$	0.9587(17)[a]	2.954(13)[a]
	0.9530(19)[b]	3.336(13)[b]
(^{Phen}L^{Me,Ph})FeBr$_2$	0.8047(13)	2.9591(25)
(^{Phen}L^{Me,iPr})FeBr$_2$	0.8095(11)	3.1539(23)
(*P^N*)FeCl$_2$ [c]	0.680(2)	2.871(4)
((SN^H-Ph$_2$)FeCl)$_2$(μ-Cl)$_2$ [d]	0.881(1)	3.080(2)
(SN^H-*i*Pr$_2$)FeCl$_2$ [d]	0.796(2)	2.998(4)
[(^{Phen}L^{Me,Ph})$_3$Fe][PF$_6$]$_2$	0.4535(12)	0.2792(19)
[(^{Quin}L^{Me,Ph})$_3$Fe][PF$_6$]$_2$	0.4642(46)	0.289(11)
(^{Phen}NNN^{Quin})$_2$Fe [e]	0.2911(6)	1.442(1)

[a] Relative area = 55.6% [b] Relative area = 44.4% [c] *P^N* = *N*-(di-*iso*-propyl)phosphino-2-aminopyridine; 298 K. Data from reference[22] [d] SN^H-Ph$_2$ = *N*-(2-pyridyl)amino(diphenylphosphine sulfide), 78 K; Data from reference[23]. SN^H-*i*Pr$_2$ = *N*-(2-pyridyl)amino(di-*iso*-propylphosphine sulfide), 78 K; Data from reference[22] [e] ^{Phen}NNN^{Quin} = *N,N*-(4-(2-*tert*-butyl)phenanthridinyl)(8-quinolinyl)amido; 10 K. Data from reference[14]

Cyclic voltammograms of ((^{Phen}L^{H,Ph})FeBr)$_2$(μ-Br)$_2$, (^{Phen}L^{Me,Ph})FeBr$_2$ and (^{Phen}L^{Me,iPr})FeBr$_2$ were collected in dichloromethane solutions containing 0.1 M [*n*Bu$_4$N][PF$_6$] electrolyte at room temperature (Figure 6a). All three complexes showed irreversible oxidation and reduction events. As with the results of their other spectral characterization (e.g. UV-Vis absorption), the cyclic voltammograms of ((^{Phen}L^{H,Ph})FeBr)$_2$(μ-Br)$_2$, (^{Phen}L^{Me,Ph})FeBr$_2$ are quite similar, again suggesting similar electronic environments in solution for both complexes. The peaks of the irreversible oxidation events, however, are shifted to lower potential for the complex of the more electron-releasing ^{Phen}L^{Me,Ph} ligand ($E_{peak,ox}$ for (^{Phen}L^{Me,Ph})FeBr$_2$: 0.63, 1.11 V; $E_{peak,ox}$ for ((^{Phen}L^{H,Ph})FeBr)$_2$(μ-Br)$_2$: 0.80, 1.40 V vs FcH$^{0/+}$), as are the peak potentials for the irreversible reduction event ($E_{peak,red}$ for (^{Phen}L^{Me,Ph})FeBr$_2$: -2.04 V; E_{peak} for ((^{Phen}L^{H,Ph})FeBr)$_2$(μ-Br)$_2$: -1.85 vs FcH$^{0/+}$). In contrast, only a single oxidation event is observed for (^{Phen}L^{Me,iPr})FeBr$_2$ at 0.77 V vs FcH$^{0/+}$. A reduction event could not be clearly resolved within the solvent window for this compound.

In comparison, the electrochemical response observed for [(^{Phen}L^{Me,Ph})$_3$Fe][PF$_6$]$_2$ and [(^{Quin}L^{Me,Ph})$_3$Fe][PF$_6$]$_2$ in acetonitrile solution was much more reversible (Figure 6b). Both complexes show a reversible Fe$^{2+/3+}$ couple at comparable potentials ([(^{Phen}L^{Me,Ph})$_3$Fe][PF$_6$]$_2$: $E_{1/2}$ = 0.82 V vs FcH$^{0/+}$; [(^{Quin}L^{Me,Ph})$_3$Fe][PF$_6$]$_2$: $E_{1/2}$ = 0.83 V vs FcH$^{0/+}$). A reversible reduction event can be also seen, again at comparable potentials ([(^{Phen}L^{Me,Ph})$_3$Fe][PF$_6$]$_2$: $E_{1/2}$ = -1.61 V vs FcH$^{0/+}$; [(^{Quin}L^{Me,Ph})$_3$Fe][PF$_6$]$_2$: $E_{1/2}$ = -1.55 V vs FcH$^{0/+}$). The slight cathodic shift to the reduction event for the more π-extended phenanthridine ligand suggests a higher energy LUMO, consistent with the blue-shifted λ_{max} for [(^{Phen}L^{Me,Ph})$_3$Fe][PF$_6$]$_2$ observed by UV-Vis absorption spectroscopy.

Oxidation of [(^{Phen}L^{Me,Ph})$_3$Fe][PF$_6$]$_2$ and [(^{Quin}L^{Me,Ph})$_3$Fe][PF$_6$]$_2$ in a spectroelectrochemical cell (Figure 7) showed the loss of the low energy peak for both complexes, which moved to higher energy with visible isosbestic points at potentials corresponding to the reversible 1e$^-$ redox couple observed by cyclic voltammetry. This is consistent with an Fe$^{2+/3+}$ redox couple that shifts the energy of an MLCT-type transition to higher energy upon removal of an electron from the metal-centred HOMO. Oxidation of the corresponding ruthenium complexes was only observed at much higher potentials, as predicted by the lack of lower energy transitions in the visible region of the UV-Vis absorption spectra for [(^{Phen}L^{Me,Ph})$_3$Ru][PF$_6$]$_2$ and [(^{Quin}L^{Me,Ph})$_3$Ru][PF$_6$]$_2$ and meaningful spectroelectrochemical data could not be obtained.

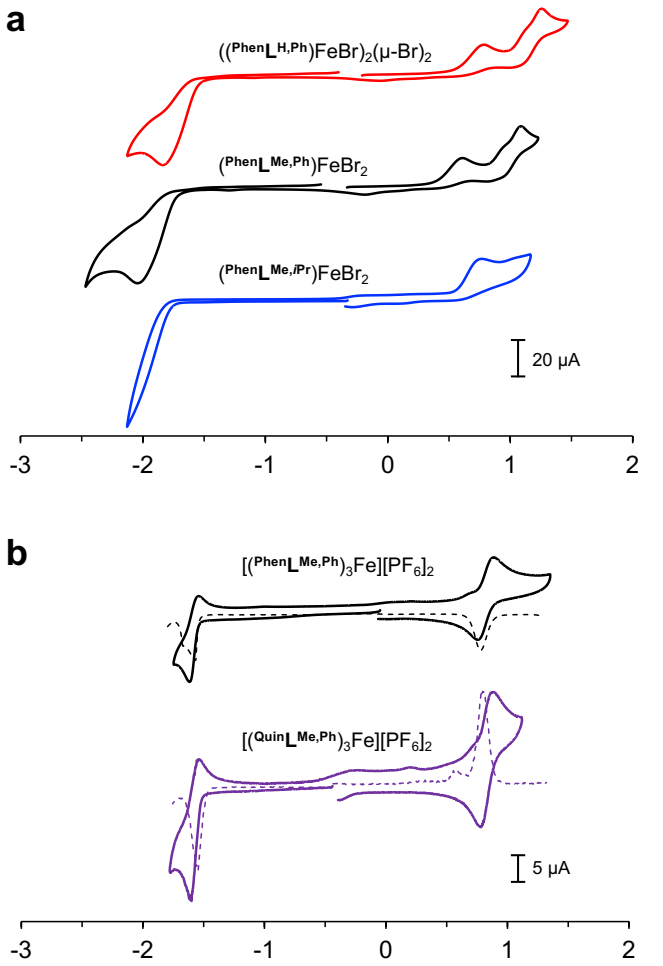

Figure 6. Cyclic voltammograms (295 K) of (a) ((^{Phen}L^{H,Ph})FeBr)$_2$(μ-Br)$_2$, (^{Phen}L^{Me,Ph})FeBr$_2$ and (^{Phen}L^{Me,iPr})FeBr$_2$ in CH$_2$Cl$_2$; and (b) cyclic voltammograms (—) and differential pulse voltammograms (---) of [(^{Phen}L^{Me,Ph})$_3$Fe][PF$_6$]$_2$ and [(^{Quin}L^{Me,Ph})$_3$Fe][PF$_6$]$_2$ in CH$_3$CN.

Computational Analysis

To more closely examine the electronic structures of [(^{Phen}L^{Me,Ph})$_3$Fe][PF$_6$]$_2$ and [(^{Quin}L^{Me,Ph})$_3$Fe][PF$_6$]$_2$ and help interpret the blue-shifted lowest energy absorption observed for the complex with the more π-extended ligand, density functional theory (DFT) and time-dependent DFT (TDDFT) simulations of the two dications were undertaken. Optimization of the ground-state structures was conducted using Cartesian coordinates from the crystal structures as the starting input (see Supporting Information for details). Calculated structural metrics were in good agreement with those obtained in the solid-state (Table S2). The molecular orbital energy level diagrams (Figure 8) show a *d*-orbital splitting consistent with a pseudo-octahedral ligand field; the HOMO, HOMO-1 and

HOMO-2 molecular orbitals represent what would be the t_{2g} set and are comprised of the d_{xz}, d_{xy} and d_{yz} orbitals collectively (see Table S3-S4 for population analysis). What would be the e_g set in a formally octahedral coordination environment, the $d_{x^2-y^2}$ and d_{z^2}, are accordingly destabilized and appear as the LUMO+3 and LUMO+4 ($[(^{Quin}L^{Me,Ph})_3Fe]^{2+}$) and LUMO+6 and LUMO+7 ($[(^{Phen}L^{Me,Ph})_3Fe]^{2+}$) with σ-anti-bonding character between Fe and the phosphines. The e_g-type orbitals lie at only slightly higher energies in $[(^{Phen}L^{Me,Ph})_3Fe]^{2+}$ vs. $[(^{Quin}L^{Me,Ph})_3Fe]^{2+}$.

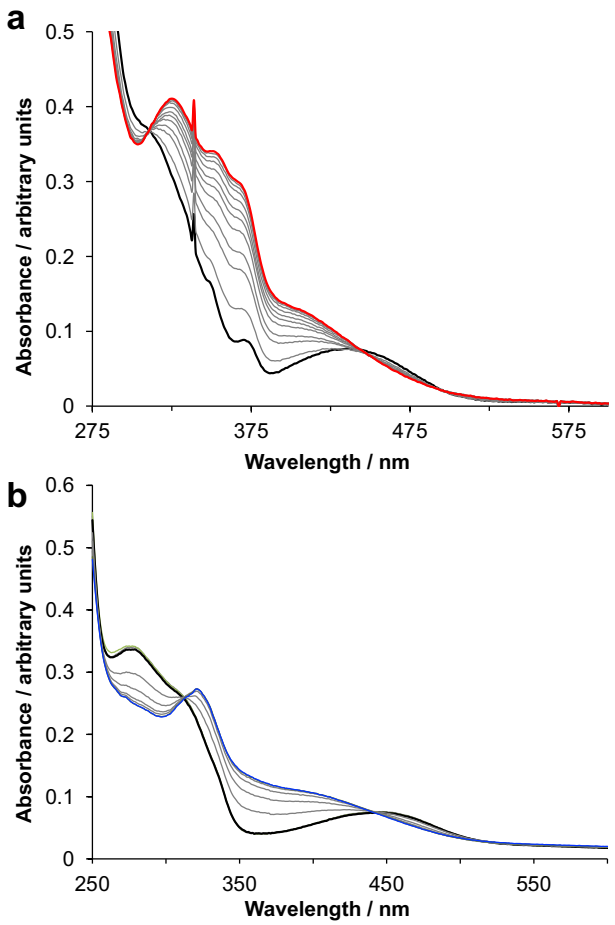

Figure 7. Absorbance spectra collected at 295 K of 0.1 M $[n\text{Bu}_4\text{N}][PF_6]$ CH_3CN solutions containing (a) $[(^{Phen}L^{Me,Ph})_3Fe][PF_6]_2$, with oxidative potentials applied from +1.0 to +1.4 V vs Ag/Ag^+; and (b) $[(^{Quin}L^{Me,Ph})_3M][PF_6]_2$, with oxidative potentials applied from +0.4 to +1.1 V vs Ag/Ag^+. For each set of traces, the solid black line indicates spectrum collected prior to the application of anodic potential.

In $[(^{Phen}L^{Me,Ph})_3Fe]^{2+}$, the three lowest energy unoccupied MOs (the LUMO, LUMO+1 and LUMO+2) have considerable orbital density localized at the C=N sub-unit of the phenanthridinyl ligand. The same three orbitals in $[(^{Quin}L^{Me,Ph})_3Fe]^{2+}$ have analogous C=N (quinolinyl) character, but with a lower degree of localization. However, the more π-extended phenanthridinyl ligand does provides three additional, low-lying, vacant, ligand-based π* orbitals (LUMO+3 through LUMO+5) compared with $[(^{Quin}L^{Me,Ph})_3Fe]^{2+}$. Population analysis indicates these orbitals are localized on the phenanthridinyl π-system and are largely comprised of the phenanthridine aryl rings. To try to trace the origin of these orbitals to what can be thought of as the benzannulation of the quinolinyl moiety in $^{Quin}L^{Me,Ph}$ to a phenanthridinyl unit in $^{Phen}L^{Me,Ph}$, we carried out charge decomposition analysis (CDA) on a $^{Phen}L^{Me,Ph}$ ligand extracted from the optimized structure of $[(^{Phen}L^{Me,Ph})_3Fe]^{2+}$, splitting the $^{Phen}L^{Me,Ph}$ ligand into its quinoline-congener and a *cis*-butadiene-type fragment. The relevant fragment orbital (FO) interactions are summarized in Figure S1. A relatively complex orbital interaction is observed to be in play between the quinolinyl and butadiene molecular fragments. Both the α- and β-orbitals indicate similar interactions, so only the α-manifold is discussed here focusing on those with FO composition ($\Theta_{m,i}$) > 10%. Overall, the π* orbital interactions between the quinolinyl α-LUMO (α-MO 87; $\Theta_{m,i}$ = 16 %) and α-LUMO+1 (α-MO 88; $\Theta_{m,i}$ = 30 %) and butadiene α-LUMO (α-MO 16; $\Theta_{m,i}$ = 33 %) appear to be responsible for the three additional π* orbitals found in $[(^{Phen}L^{Me,Ph})_3Fe]^{2+}$. Thus, the most significant interaction is a cooperative one between two vacant orbitals.

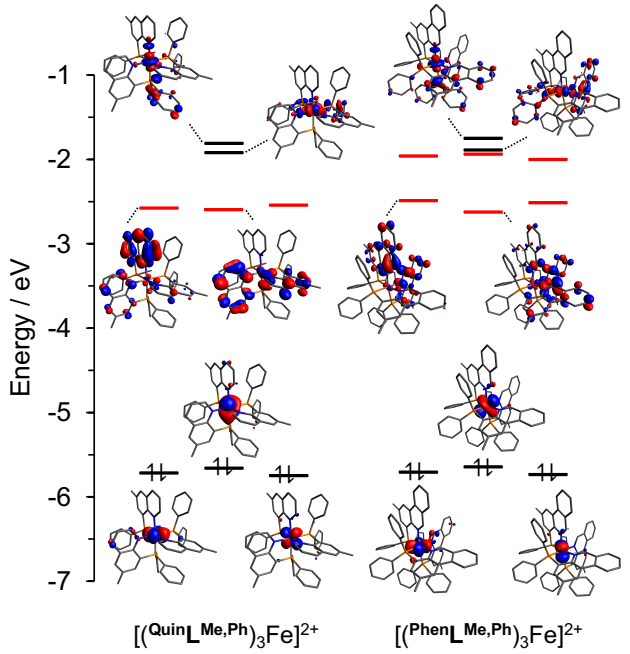

Figure 8. Selected ground state MO energy diagram and orbitals (isosurface = 0.04) for $[(^{Quin}L^{Me,Ph})_3Fe]^{2+}$ and $[(^{Phen}L^{Me,Ph})_3Fe]^{2+}$ (SMD-TPSSh/def2-SVP//SMD-B3LYP-D3(BJ)/def2-SVP). Vacant, acceptor ligand-based π* orbitals are highlighted in red. Fragment contributions to selected MOs are tabulated in Tables S3-S4.

The above is reminiscent of the symmetry arguments made by Hanson *et al.*[8] in explaining the red-shift of both absorption and emission observed for a Pt(II) chloride complex of 1,3-*bis*(2-pyridylimino)benz(*e*)isoindolate compared with from an analogous complex of 1,3-*bis*(2-pyridylimino)isoindolate. In that case, however, the primary impact of benzannulation was on the frontier orbitals. Here, despite the expanded π-system in $[(^{Phen}L^{Me,Ph})_3Fe]^{2+}$, the calculated HOMO-LUMO gaps in $[(^{Quin}L^{Me,Ph})_3Fe]^{2+}$ (3.06 eV) and $[(^{Phen}L^{Me,Ph})_3Fe]^{2+}$ (3.02 eV) are not significantly different and indeed, in absolute terms, appear to contradict the hypsochromic shift observed for $[(^{Phen}L^{Me,Ph})_3Fe][PF_6]_2$. The additional vacant orbitals do have a significant impact on the observed absorption spectrum of $[(^{Phen}L^{Me,Ph})_3Fe]^{2+}$, however, as revealed by TDDFT. The

electronic excitation with a dominant HOMO→LUMO contribution (State 4 in both $[(^{Quin}L^{Me,Ph})_3Fe]^{2+}$ and $[(^{Phen}L^{Me,Ph})_3Fe]^{2+}$; Figures S2-S3) is effectively turned-off in $[(^{Quin}L^{Me,Ph})_3Fe]^{2+}$ (f_{osc} = 0.004; Table S5), but gains in intensity in $[(^{Phen}L^{Me,Ph})_3Fe]^{2+}$ (f_{osc} = 0.025; Table S6). This contrasts with the behaviour of Group 10 metal complexes supported by *bis*(8-quinolinyl)amido, (8-quinolinyl)(4-phenanthridinyl)amido and *bis*(4-phenanthridinyl)amido ligands.[6] There, benzannulation has the opposite effect – the HOMO→LUMO transition has significant oscillator strength for the complex with the smallest π-system (*i.e.*, supported by the *bis*(8-quinolinyl)amido ligand) and is essentially dark for the complex of with the largest π-system (*i.e.*, supported by a *bis*(4-phenanthridinyl)amido scaffold).

TDDFT simulations of the electronic absorption spectra furthermore predict stronger vertical excitations (f_{osc} > 0.05) at lower energy (2.76-2.87 eV; see Table S5) for $[(^{Quin}L^{Me,Ph})_3Fe]^{2+}$ compared with $[(^{Phen}L^{Me,Ph})_3Fe]^{2+}$ (2.81-2.92 eV; see Table S6). This change in the strength of excitations at low energy appears to be one of the causes of the counter-intuitive blue-shifted λ_{max} for the complex bearing the larger ligand π-system. Overall, in both systems, TDDFT assigned the lowest energy absorption manifold to have significant metal-to-ligand charge transfer character (MLCT; see Figures S4-S5 for electron-hole density maps). The acceptor orbitals in both cases are ligand-centred with $\pi^*_{C=N}$ character (LUMO to LUMO+2) for both cations. Formally metal-centred (MC) excited states gain intensity (f_{osc} > 0.01) at slightly higher energy than the MLCT states. This suggests low-lying MC states could provide a non-radiative deactivation pathway for these complexes.[25] Indeed, no luminescence could be observed at room temperature from solutions of $[(^{Phen}L^{Me,Ph})_3Ru][PF_6]_2$ nor $[(^{Quin}L^{Me,Ph})_3Ru][PF_6]_2$, consistent with observations of related complexes.[20]

The additional π* orbitals of $[(^{Phen}L^{Me,Ph})_3Fe]^{2+}$ discussed above lie below the formally e_g orbital set and are predicted to participate in excitations at higher energies (E > 3.2 eV; λ < 390 nm). These additional π* orbitals have a considerable impact on the electronic transitions in this region of the spectrum. The formally MC states ($^1S_{13\text{-}15}$, Table S6) of $[(^{Phen}L^{Me,Ph})_3Fe]^{2+}$ are higher in intensity than those of $[(^{Quin}L^{Me,Ph})_3Fe]^{2+}$ ($^1S_{13}$, Table S5), as electron-hole pair contributions of MLCT character considerably mix with these states. The additional electron-hole pair contributions can be attributed to the 't_{2g}' donor and the additional π* acceptor orbitals (LUMO+3 to LUMO+5). Additional MLCT states, with the three new π* orbitals serving as acceptor orbitals, dominate the near-UV region of the spectrum. Consequently, absorbance in this region becomes more significant than in $[(^{Quin}L^{Me,Ph})_3Fe]^{2+}$, consistent with the increased absorptive cross-section in the near-UV region. Increasing the molar absorptivity across the visible region of the electromagnetic spectrum is particularly important in the design of light harvesting dyes, for which expansion of the π-system of the ligand ($[(^{Quin}L^{Me,Ph})_3Fe]^{2+}$ vs $[(^{Phen}L^{Me,Ph})_3Fe]^{2+}$) through benzannulation provides such a means.

It is also instructive to compare the observation of a blue-shifted λ_{max} for $[(^{Phen}L^{Me,Ph})_3Fe][PF_6]_2$ compared with $[(^{Quin}L^{Me,Ph})_3Fe][PF_6]_2$ with other transition metal complexes of pairs of phenanthridinyl and quinolinyl-containing ligands similarly related by ligand benzannulation. The counter-intuitive shift of the lowest energy absorption to higher energy for the complex comprised of a ligand with a larger π-system, $[(^{Phen}L^{Me,Ph})_3Fe][PF_6]_2$, stands in contrast to trends observed for Cu(I) complexes of related quinoline/phenanthridine-based *P^N* ligands.[9] There, a bathochromic shift of the lowest energy MLCT absorptions is observed for dimeric $(P^N)_2Cu_2X_2$ complexes of $^{Phen}L^{H,Ph}$ compared with those of $^{Quin}L^{H,Ph}$. In comparison, Group 10 complexes of pincer-like tridentate *N^N^N* ligands bearing either quinolinyl or phenanthridinyl arms show nearly identical λ_{max} values that were invariant in the face of increasing π-extension.[6] Isoenergetic lowest energy absorptions were also observed for pseudo-octahedral $Re(CO)_3X$ (X = Br, Cl) complexes of bidentate (4-amino)phenanthridine and (8-amino)quinoline ligands.[26]

In each of these scenarios the different impacts of ligand benzannulation cannot be solely connected to the (de)stabilization of the frontier orbitals, as suggested by some other studies.[8,27,5] Rather, the particular benzannulation of quinoline to phenanthridine (3,4-benzoquinoline) can also strongly impact the oscillator strengths of the lowest energy transitions. This can have a less intuitive influence on the overall absorption profile. Changing from quinoline to phenanthridine in the aforementioned Group 11 $(P^N)_2Cu_2X_2$ series has a predictable (if small) effect – the lowest energy absorption tails to yet longer wavelengths.[9] In comparison, Group 10 complexes of tridentate phenanthridine/quinoline-containing ligands have nearly isoenergetic λ_{max} values.[6] There, while benzannulation does lower the energy of the LUMO, the HOMO-LUMO transition is effectively turned-off in phenanthridinyl-containing complexes in favor of higher energy HOMO-LUMO+1 transitions. Quinoline to phenanthridine π-extension has a more pronounced impact on the phosphorescence from Pt(II) congeners of these same ligands, which is blue-shifted in complexes of the benzannulated phenanthridinyl-based complexes, a phenomenon ascribed to the enhanced rigidity of the larger *N*-heterocyclic donor arms.[7] In yet another twist, the LUMO energies of both phenanthridinyl and quinolinyl supported $(N^N)Re(CO)_3X$ complexes are calculated to lie at nearly identical energies.[26] In that case, the major difference observed was in the intensity of λ_{max}, attributed to a more purely MLCT-type excitation at lower energy for the phenanthridine-supported complex compared with the quinoline-ligated analog, similar to the findings reported here. Collectively, these results reveal that ligand benzannulation can influence orbital energies, oscillator strengths of transitions and structural rigidity, with a range of consequences for photophysical properties of coordination complexes.

Conclusions

The synthesis and characterization of a series of Group VIII metal coordination complexes of bidentate, *N*-heterocycle-based *P^N* ligands bearing diaryl or dialkyl phosphine donors and π-extended phenanthridine (3,4-benzoquinoline; $^{Phen}L^{R,R'}$) (R = H, R' = Ph; R = Me, R' = Ph; R = Me, R' = *i*Pr) or quinoline

(^{Quin}L^{Me,Ph}) *N*-heterocycles is reported. Iron halide complexes of the phenanthridine-containing ligands ^{Phen}L^{Me,R} (R = Ph, *i*Pr) were characterized as tetrahedral monomers (*P^N*)$FeBr_2$ in the solid-state. The corresponding iron dibromide complex of ^{Phen}L^{H,Ph} instead crystallized as a distorted trigonal bipyramidal dimer ((*P^N*)$FeBr)_2(\mu\text{-}Br)_2$. All complexes exhibited high-spin paramagnetic character as solids and in solution. The Mössbauer spectrum of ((^{Phen}L^{H,Ph})$FeBr)_2(\mu\text{-}Br)_2$ was well described by two Fe environments, one of which was assigned as tetrahedral and monomeric by comparison with the spectrum of (^{Phen}L^{Me,Ph})$FeBr_2$. The solution-state electronic environment of ((^{Phen}L^{H,Ph})$FeBr)_2(\mu\text{-}Br)_2$ examined by electrochemistry and electronic absorption spectroscopy was also remarkably similar to that of (^{Phen}L^{Me,Ph})$FeBr_2$, suggesting a likely monomer-dimer equilibrium at play in solution. In comparison, the *tris*-ligated octahedral $[(P\text{^}N)_3M]^{2+}$ cations (M = Fe, Ru) are low-spin diamagnets. For the pseudo-octahedral Fe(II) complexes, the impact of π-extension is evident when comparing the lowest energy absorption bands of $[(^{Phen}L^{Me,Ph})_3Fe][PF_6]_2$ and $[(^{Quin}L^{Me,Ph})_3Fe][PF_6]_2$ in solution. Contrary to the conventional assumptions regarding π-extension, a hypsochromic shift was observed for π-extended (phenanthridinyl) phosphine Fe(II) complex. Overall, our findings further emphasize the nuances that have emerged in broader investigations into structure-property relationships of coordination complexes of quinoline vs. phenanthridine-containing multidentate ligands.

Author Contributions

The manuscript was written through contributions of all authors. All authors have given approval to the final version of the manuscript.

Conflicts of interest

There are no conflicts to declare.

Acknowledgements

We gratefully acknowledge the Natural Sciences Engineering Research Council of Canada for Discovery Grants to DEH (RGPIN-2014-03733) and JvL (RGPIN-2018-05012); the Canada Foundation for Innovation and Research Manitoba for an award in support of an X-ray diffractometer (CFI #32146); the University of Manitoba for the Bert & Lee Friesen Graduate Scholarship (IBL) and GETS/SEGS support (RM, JDB, IBL); and Compute Canada for computational resources. Prof. V.N. Nemykin is thanked for access to spectroelectrochemical equipment and Prof. S. Kroeker and A. Krishnamurthy are thanked for use of and assistance with a solid-state magnetic susceptibility balance.

References

1 Z. Li and W. Sun, *Dalton Trans.*, 2013, **42**, 14021–14029.
2 Z. Li, P. Cui, C. Wang, S. Kilina and W. Sun, *J. Phys. Chem. C*, 2014, **118**, 28764–28775.
3 A. Tsuboyama, H. Iwawaki, M. Furugori, T. Mukaide, J. Kamatani, S. Igawa, T. Moriyama, S. Miura, T. Takiguchi, S. Okada, M. Hoshino and K. Ueno, *J. Am. Chem. Soc.*, 2003, **125**, 12971–12979.
4 A. Bossi, A. F. Rausch, M. J. Leitl, R. Czerwieniec, M. T. Whited, P. I. Djurovich, H. Yersin and M. E. Thompson, *Inorg. Chem.*, 2013, **52**, 12403–12415.
5 B. Liu, L. Lystrom, S. Kilina and W. Sun, *Inorg. Chem.*, 2017, **56**, 5361–5370.
6 P. Mandapati, P. K. Giesbrecht, R. L. Davis and D. E. Herbert, *Inorg. Chem.*, 2017, **56**, 3674–3685.
7 P. Mandapati, J. D. Braun, C. Killeen, R. L. Davis, J. A. G. Williams and D. E. Herbert, *Inorg. Chem.*, 2019, **58**, 14808–14817.
8 K. Hanson, L. Roskop, P. I. Djurovich, F. Zahariev, M. S. Gordon and M. E. Thompson, *J. Am. Chem. Soc.*, 2010, **132**, 16247–16255.
9 R. Mondal, I. B. Lozada, R. L. Davis, J. A. G. Williams and D. E. Herbert, *Inorg. Chem.*, 2018, **57**, 4966–4978.
10 R. Mondal, I. B. Lozada, R. L. Davis, J. A. G. Williams and D. E. Herbert, *J. Mater. Chem. C*, 2019, **7**, 3772–3778.
11 T. Schlotthauer, G. A. Parada, H. Goerls, S. Ott, M. Jaeger and U. S. Schubert, *Inorg. Chem.*, 2017, **56**, 7720–7730.
12 V. Sicilia, S. Fuertes, A. Martin and Adrian. Palacios, *Organometallics*, 2013, **32**, 4092–4102.
13 B. Jiang, Y. Gu, J. Qin, X. Ning, S. Gong, G. Xie and Chuluo. Yang, *J. Mater. Chem. C*, 2016, **4**, 3492–3498.
14 J. D. Braun, I. B. Lozada, C. Kolodziej, C. Burda, K. M. E. Newman, J. van Lierop, R. L. Davis and D. E. Herbert, *Nat. Chem.*, 2019, **11**, 1144–1150.
15 P. Mandapati, J. D. Braun, I. B. Lozada, J. A. G. Williams and D. E. Herbert, *Inorg. Chem.*, 2020, **59**, 12504–12517.
16 R. Mondal, P. K. Giesbrecht and D. E. Herbert, *Polyhedron*, 2016, **108**, 156–162.
17 A. W. Addison, T. N. Rao, J. Reedijk, J. van Rijn and G. C. Verschoor, *J. Chem. Soc., Dalton Trans.*, 1984, 1349–1356.
18 E. M. Schubert, *J. Chem. Educ.*, 1992, **69**, 62.
19 G. A. Bain and J. F. Berry, *J. Chem. Educ.*, 2008, **85**, 532.
20 T. Suzuki, T. Kuchiyama, S. Kishi, S. Kaizaki, H. D. Takagi and M. Kato, *Inorg. Chem.*, 2003, **42**, 785–795.
21 A. A. Tsaturyan, A. P. Budnyk and C. Ramalingan, *ACS Omega*, 2019, **4**, 10991–11003.
22 C. Holzhacker, C. M. Standfest-Hauser, M. Puchberger, K. Mereiter, L. F. Veiros, M. J. Calhorda, M. D. Carvalho, L. P. Ferreira, M. Godinho, F. Hartl and K. Kirchner, *Organometallics*, 2011, **30**, 6587–6601.
23 C. Holzhacker, M. J. Calhorda, A. Gil, M. D. Carvalho, L. P. Ferreira, K. Mereiter, B. Stöger, E. Pittenauer, G. Allmaier and K. Kirchner, *Polyhedron*, 2014, **81**, 45–55.
24 P. Gütlich, E. Bill and A. X. Trautwein, in *Mössbauer Spectroscopy and Transition Metal Chemistry: Fundamentals and Applications*, eds. P. Gütlich, E. Bill and A. X. Trautwein, Springer Berlin Heidelberg, Berlin, Heidelberg, 2011, pp. 73–135.
25 O. S. Wenger, *Chem. – Eur. J.*, 2020, **25**, 6043–6052.
26 S. Gaire, R. J. Ortiz, B. R. Schrage, I. B. Lozada, P. Mandapati, A. J. Osinski, D. E. Herbert and C. J. Ziegler, *J. Organomet. Chem.*, 2020, **921**, 121338.
27 S. M. Barbon, V. N. Staroverov and J. B. Gilroy, *J. Org. Chem.*, 2015, **80**, 5226–5235.